Impact of Photon Absorption on the Electronic Properties of *p*-Coumaric Acid Derivatives of the Photoactive Yellow Protein Chromophore

Lavanya L. Premvardhan,*,† Francesco Buda,‡ Michael A. van der Horst,§ Daniel C. Lührs,† Klaas J. Hellingwerf,§ and Rienk van Grondelle†

Department of Biophysics and Physics of Complex Systems, Division of Physics and Astronomy, Faculty of Sciences, Vrije Universiteit, De Boelelaan 1081, 1081 HV Amsterdam, The Netherlands, Leiden Institute of Chemistry, Leiden University, Einsteinweg 55, 2300 RA Leiden, The Netherlands, and Laboratory for Microbiology, Swammerdam Institute for Life Sciences, Universiteit van Amsterdam, Nieuwe Achtergracht 166, 1018 WV Amsterdam, The Netherlands

Received: November 13, 2003; In Final Form: January 30, 2004

The changes in the electrostatic properties, between the ground and excited state, of thiomethyl *p*-coumaric acid (TMpCA) and its sterically hindered derivative, thiomethyl-7-hydroxy-coumarin-3-carboxylic acid (TM7HC), have been determined at 77 K using Stark spectroscopy, to better understand the origin of the photoinduced charge motion observed in these chromophores in the native photoactive yellow protein (PYP) environment. Excitation of the anionic chromophores produce changes in the permanent dipole moment ($|\Delta\vec{\mu}|$) of 25 (TMpCA-a) and 15 D (TM7HC-a), which are significantly larger than the $|\Delta\vec{\mu}|$'s measured in the neutral species: 9 (TMpCA-n) and 6 D (TM7HC-n). However, the similarity of the $|\Delta\vec{\mu}|$'s between the anions and the corresponding de-protonated cofactors in the native protein environment implicates the intrinsic electronic properties of the chromophore for the photoreactivity of the initially excited species in the PYP photocycle. Furthermore, the results for the neutral species suggest that, if the cofactor in the protein were to be protonated in the ground state, photon absorption would induce a much smaller degree of charge motion. The implications of these distinct differences in the measured electrostatic properties are discussed in the context of facilitating and/or preventing the twisting of the chromophore and its relevance to the PYP photocycle. Ab initio (time dependent density functional, TDDFT) calculations on these systems yield quite accurate values for the electronic transition energies, and the molecular orbitals that contribute to these transitions provide an insight into the reactivity of the excited-state species. However, the changes in the permanent dipole moments associated with these transitions are underestimated, particularly in the anions, both from Configuration Interactions − Singles and Restricted Open-shell Kohn−Sham calculations.

Introduction

Thio-methyl *para*-coumaric acid (TMpCA) is a model chromophore used to study the properties of the cofactor in wild-type photoactive yellow protein (WT-PYP). This protein is implicated in the blue-light negative-phototactic response of the bacterium *Halorhodospira halophila*,[1] thereby protecting it from harmful exposure to blue light.[2] In PYP, the active cofactor, identified as 4-hydroxycinnamyl cysteine thioester, undergoes a photocycle, which is ultimately linked to signal transduction in the organism.[3] Excitation of the ground-state species, pG, initiates a photocycle during which a number of intermediates, associated with the important trans−cis isomerization of the cofactor,[4−7] are generated.[3,4,8] Our previous investigation of WT-PYP,[9] using Stark spectroscopy, showed that excitation of pG induced a large degree of charge motion and produced a change in dipole moment, $|\Delta\vec{\mu}|$, of 26 D, much larger than that measured even in retinal proteins.[10] The accompanying change in the charge distribution of the initially excited species was suggested to increase the single bond character of the double bond around which isomerization occurs. Thus, the twisting of the chromophore is facilitated in the excited-state triggering the PYP photocycle.[9] Therefore, we have undertaken the current study on model chromophores, similar to the cofactors previously studied in the protein environment, to better understand the phenomenon of light-induced charge motion in PYP. Indeed, the formation of charged species has also been shown to be important in subsequent events during the PYP photocycle.[11] In addition to WT-PYP, we also studied the native apo-protein reconstituted with the chromophore prevented from undergoing trans−cis isomerization, produced by effectively "locking" the C7−C8 double bond (L-PYP in ref 9). Here, we have used the anion TMpCA-a, as the model chromophore for the wild-type species and anionic thiomethyl-7-hydroxy-coumarin-3-carboxylic acid, TM7HC-a, (also referred to as TML in ref 12) as the model for the chromophore in L-PYP (Scheme 1).

In the past, free *p*-coumaric acid (pCA) has been used to characterize the properties of the cofactor in WT-PYP[13,14] and has provided much useful insight about the photophysical properties of WT-PYP. TMpCA-a is however presumed to be a better substitute because, the anionic oxy group in pCA is not isoelectronic with the thiol group in the protein, and in pH 10 buffer solutions, pCA is doubly de-protonated versus the single de-protonation in TMpCA-a and the cofactor in the protein. By comparing the electronic properties of TMpCA-a

* To whom correspondence should be addressed. E-mail: lp2f@nat.vu.nl.
† Vrije Universiteit.
‡ Leiden University.
§ Universiteit van Amsterdam.

10.1021/jp037469b CCC: $27.50
Published on Web 03/26/2004

SCHEME 1: Chemical Structures of Chromophores[a]

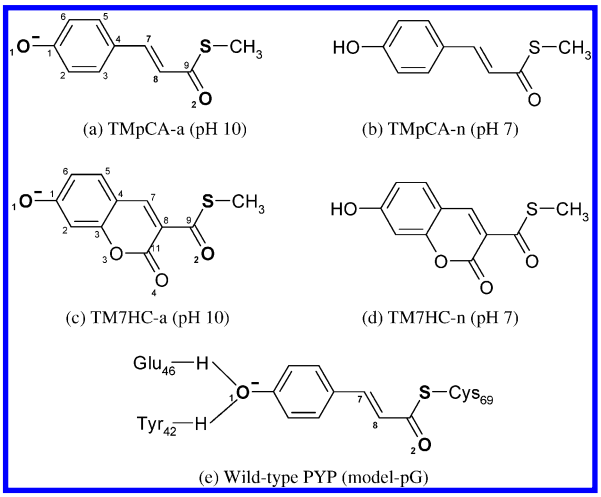

[a] The chemical structures of (a) anionic TMpCA at pH 10: TMpCA-a (b) neutral TMpCA at pH 7: TMpCA-n (c) anionic TM7HC at pH 10: TM7HC-a (d) neutral TM7HC at pH 7: TM7HC-n (e) ground-state wild-type PYP: model-pG (The positive Arg52 counterion and threonine50 residue are not shown here).

and TM7HC-a with those of the protein-embedded chromophores, we can determine to what extent the protein environment and the configurational alterations that prevent isomerization affect the photophysics of this system in the first few femtoseconds after light absorption. In addition, by comparing the properties of TMpCA-a to those of TM7HC-a, we can establish whether either of these cofactors is more strongly coupled to, or affected by, the protein environment. That is, which of the two model chromophores behaves most similarly to the corresponding cofactor in the protein, or conversely, for which of these two systems does the protein environment more strongly affect the properties of the chromophore? To this end, we have measured the change in the absorption spectrum induced in the presence of an external electric field, the Stark effect, to *quantitate* the extent of charge motion on photon absorption. Stark spectroscopy has been used to study many biological pigment−protein complexes,[9,15,16] as well as chromophores in the condensed phase, including coumarins,[17] to obtain important information about their photoreactivity. In particular, it is useful for identifying charge-transfer transitions. The electrostatic parameters that allow us to study these effects, and that can be determined from the Stark signal, are the change in the permanent dipole moment, $|\Delta\vec{\mu}|$, and the change in polarizability, $\overline{\Delta\alpha}$. Here, they are used to understand the implications of electronic charge displacement associated with photon absorption by TMpCA and TM7HC, within and outside the protein, and due to protonation.

Besides the many experiments performed on PYP in the protein environment and on model chromophores, particularly on pCA,[18−20] electronic-structure calculations have been used to elucidate its essential photophysical properties.[18−23] The electronic and vibronic transition energies of various PYP intermediates, including the ground-state dark species, pG, and the cis isomer, pR, have been calculated to characterize the changing potential energy surface of the PYP photocycle, with much attention being paid to the (barrier to) trans−cis isomerization. Both time-dependent density functional theory (TD-DFT)[19,21,23] and multi-configuration second-order perturbation theory (MS−CASPT2)[18,20] have been used. Although ground-state properties can be evaluated with high accuracy using DFT, accurate calculations of excited-state properties still pose a challenge. Here we use linear response calculations within TDDFT,[24] generally comparable in accuracy to computationally more demanding wavefunction-based methods,[25] to calculate the electronic excitation energies and to characterize these transitions. In addition, partial atomic charges and permanent dipole moments and polarizabilites in the ground and excited states, which have not been reported before, have been calculated for the systems shown in Scheme 1 and are directly compared to these electrostatic properties estimated from the Stark experiments.

We have focused our attention on TMpCA-a as it is used as the model for the biologically important cofactor in PYP. However, the electronic properties of the neutral chromophores, TMpCA-n and TM7HC-n, are also of interest. These molecules, which fall into the family of classical solvatochromic probes such as the coumarin laser dyes, have a strong nonlinear optical response and can be potentially exploited for the construction of optoelectronic devices when doped into polymer films.[26] Indeed, the comparatively large polarizability changes measured here, particularly in TM7HC-n, are indicative of the nonlinear properties of these molecules. Moreover, the absorption bands of these molecules are quite sensitive to the changing polarity of the environment, underscoring their potential to be used as polarity probes[27] and, in addition, to model the solvation dynamics of dipolar solutes in a solvent environment.[28] This is particularly true for the more rigid TM7HC-n as it is less susceptible to generating multiple ground-state conformers that can, in general, complicate the analysis of the spectroscopic signature of the molecule.

Materials and Methods

Sample Preparation and Apparatus. The synthesis of anionic and neutral TMpCA and TM7HC are described in the Supporting Information. TMpCA and TM7HC were individually dissolved in 40 mM CAPS buffer solution at pH 10 to produce buffered solutions of the corresponding anions. (Protein solutions are buffered at neutral pH, but the cofactors in the protein pocket are de-protonated in the ground state.) We note that high buffer capacity was required, particularly in the case of TM7HC-a, to ensure that the chromophores were de-protonated. Glycerol-buffer solutions were made in a ratio of 55/45 (v/v) to generate the glasses at low temperature. Since TM7HC-n was not soluble in Tris buffer at pH 7, to make the comparison of the electronic properties between the neutral molecules consistent, a common medium in which they both dissolve, in this case methyl tetrahydrofuran (MeTHF), was used as the solvent. To ensure that good-quality glasses are produced at 77 K, the MeTHF is refluxed (1−2 h) and distilled to ensure that it is dry. The solution is contained in a shallow well, created with either double-sided sticking tape (glycerol-buffer solutions), between 95 and 100 μm thick, or Kapton tape (MeTHF solutions) between a pair of semi-transparent inconel coated quartz slides (Melles Griot, 0.3 ND filters) of ≈55 μ thickness. The OD of each individual sample cell was between 0.2 and 0.8. Details of the experimental setup are available in ref 9.

Stark Effect. The field-induced change of the main absorption bands of the chromophores are analyzed using the Liptay formalism.[29] The effect of the electric field on the absorption spectrum, $A(\tilde{\nu})$, of an ensemble of molecules is measured by determining the difference in the intensity of the light transmitted through the sample in the presence of an applied field. This change in the absorbance ($\Delta A(\tilde{\nu})$), or molar extinction coefficient, averaged over all orientations, is given by

$$-\Delta A(\tilde{\nu}) = \vec{F}_{\text{eff}}{}^2\left[a_\chi A(\tilde{\nu}) + \frac{b_\chi \tilde{\nu}}{15h}\left\{\frac{\partial}{\partial\tilde{\nu}}\left(\frac{A(\tilde{\nu})}{\tilde{\nu}}\right)\right\} + \frac{c_\chi \tilde{\nu}}{30h^2}\left\{\frac{\partial^2}{\partial\tilde{\nu}^2}\left(\frac{A(\tilde{\nu})}{\tilde{\nu}}\right)\right\}\right] \quad (1)$$

$\Delta A(\tilde{\nu})$, a function of the wavenumber, $\tilde{\nu}$, is proportional to the square of the effective field, $\vec{F}_{\text{eff}}$, at the site of the solute, and to the weighted sum of the absorption function, and the first and second derivatives of the unperturbed (field-free) absorption spectrum. χ is the angle between the applied AC electric-field vector and the electric-field vector of the polarized light. The molecular electronic properties, which are independent of molecular orientations, can be obtained when χ is set at the magic angle (54.7°). From $b_{54.7}$, we can determine the average change in the electronic polarizability ($\overline{\Delta\alpha}$) of the system, a scalar quantity that is one-third the trace of the change in the second-rank polarizability tensor, $\Delta\underline{\underline{\alpha}}$, ($1/3\text{Tr}(\Delta\underline{\underline{\alpha}}) = 1/3(\Delta\alpha_{xx} + \Delta\alpha_{yy} + \Delta\alpha_{zz})$). The magnitude of the change in permanent dipole moment, $|\Delta\vec{\mu}|$, is proportional to $c_{54.7}$, often the major component of the Stark signal. The experimental measurement only permits the estimation of the magnitude, and not the sign, of the change in dipole moment and the absolute value symbol is included to make this distinction. With χ set at 90°, we can also determine the angle between the transition moment, $\hat{m}$, and $|\Delta\vec{\mu}|$, from $|\hat{m}\cdot\Delta\vec{\mu}|$, and the change in polarizability along the transition moment, $\Delta\alpha_m$. The value of $\Delta\alpha_m$ is a measure of the extent to which the molecule is polarizable in the direction of $\hat{m}$ and the anisotropy in the change in charge distribution of the molecule. To determine $|\hat{m}\cdot\Delta\vec{\mu}|$ and $\Delta\alpha_m$ accurately, it is important to have very good quality fits both at $\chi = 55$ and 90°. Therefore, we have reported $|\hat{m}\cdot\Delta\vec{\mu}|$ and $\Delta\alpha_m$ only for the neutral molecules because the fits to these Stark spectra are of much better quality (evident from the residuals) than for the anions. A more detailed explanation for the relationship between the coefficients of the derivatives, a_χ, b_χ, and c_χ to the molecular parameters are available in refs 9, 15, and 17.

The angle between the electric field and the electric field vector of the light beam, χ, is effectively set at the magic angle, 54.7°, by setting the external angle, θ_{ext}, between the sample and the incoming light beam using Snell's law to account for the refractive indices of both liquid nitrogen (1.28) and the sample environment (glycerol−buffer glass or MeTHF).[15] Variation in the external angle by ±5° accounts for less than 5% variation in an individual experimental measurement (an error of ± 0.1 in the estimated refractive index). The coefficients, a_χ, b_χ, and c_χ, are extracted by means of a linear least-squares (LLSQ) fit of the electro-absorption signal to the sum of the three terms in eq 1. All of the Stark spectra have been smoothed using a combination of polynomial filtering and a sliding-average mean method. The absorption spectra are fit to a sum of three to five gaussians using a simplex algorithm to generate smooth derivatives. The experimental electronic parameters reported in Tables 1 and 2 are the average of at least three independent experiments. The values of $\overline{\Delta\alpha}$ and $|\Delta\vec{\mu}|$ have not been corrected for the enhancement of the applied external field arising from the polarization of the solvent, i.e., $\vec{F}_{\text{eff}}$, is the product of the external applied field, $\vec{F}_{\text{ext}}$, and the cavity-field factor, f_c ($\vec{F}_{\text{eff}} = f_c \times \vec{F}_{\text{ext}}$).[15] It is difficult to determine f_c in a solute cavity that must be modeled to account for the shape of the molecule,[15] and for which we must be able to determine the vectorial components of the dipole moments and polarizabilites. Therefore, the experimental values of $\overline{\Delta\alpha}$ are reported in $\text{Å}^3/f_c^2$ and $|\Delta\vec{\mu}|$ in Debye/f_c.[31]

TABLE 1: Experimental and Calculated Electronic Properties[a] of TMpCA-a and TM7HC-a

	TMpCA-a	TM7HC-a
(i) $\tilde{\nu}_{\max}$ ($\lambda_{\max}$) buffer (298 K)	26040 (384)	23750 (421)
(ii) $\tilde{\nu}_{\max}$ ($\lambda_{\max}$) Gly/buffer (298 K)	25710 (389)	23590 (424)
(ii)$\tilde{\nu}_{\max}$ ($\lambda_{\max}$) Gly/buffer (77 K)	26390 (380)	23870 (419)
(iii) $\tilde{\nu}_{\max}$ ($\lambda_{\max}$) $S_0 \rightarrow S_2$ TDDFT	24876 (402)	24390 (410)
μ_{gs}^{gas} DFT/ROKS (CIS)	7.2 (8.2)	7.7 (8.9)
μ_{es}^{gas} DFT/ROKS (CIS)	3.4 (6.1)	4.9 (8.0)
$\overline{\lvert\Delta\vec{\mu}\rvert}$ (D/f_c)	26 ± 1	15 ± 2
$\overline{\Delta\alpha}$ ($\text{Å}^3/f_c^2$)	420 ± 70	250 ± 50

[a] The maxima of the transition energies ($\tilde{\nu}_{\max}$) of the anions, TMpCA-a and TM7HC-a in the condensed phase are reported in wavenumber (cm^{-1}) and in nanometers in parentheses ($\lambda_{\max}$), in (i) CAPS Buffer at pH 10, (ii) Gly/Buffer solutions (55/45 v/v of glycerol to CAPS buffer), and (iii) TDDFT calculations of the first allowed transition ($S_0 \rightarrow S_2$). The gas-phase values for the ground- and excited-state dipole moments, μ_{gs}^{gas} and μ_{es}^{gas}, respectively, from DFT/ROKS calculations are included, with the CIS values in parentheses. $\overline{|\Delta\vec{\mu}|}$ and $\overline{\Delta\alpha}$ are the difference dipole moment and polarizability, respectively, between the ground and excited state for the transition at 380 nm for TMpCA-a and at 419 nm for TM7HC-a. $\overline{|\Delta\vec{\mu}|}$ includes an enhancement due to the cavity field, f_c, and $\overline{\Delta\alpha}$ to f_c^2 (see Materials and Methods).

TABLE 2: Experimental and Calculated Electronic Properties[a] of TMpCA-n and TM7HC-n

	TMpCA-n		TM7HC-n	
	exptl	CIS	exptl	CIS
μ_{gs}^{gas}		3.1		6.1
μ_{es}^{gas}		5.9		7.2
α_{gs}^{gas}		21		22
$\overline{\lvert\Delta\vec{\mu}\rvert}$ (D/f_c)	9.0 ± 0.3	4.1	6.1 ± 0.9	2.6
$\overline{\Delta\alpha}$ ($\text{Å}^3/f_c^2$)	62 ± 12	10	120 ± 30	7.6
$\lvert\hat{m}\cdot\Delta\vec{\mu}\rvert/\lvert\Delta\vec{\mu}\rvert$	0.82 ± 0.10	0.99	0.97 ± 0.08	0.99
$\Delta\alpha_m$	160 ± 20	30	350 ± 30	23

[a] The ground- and excited-state dipole moments, μ_{gs}^{gas} and μ_{es}^{gas}, respectively, and the ground-state polarizability, α_{gs}^{gas}, are estimated from CIS calculations (see Materials and Methods) for TMpCA-n and TM7HC-n. The experimental values of $\overline{|\Delta\vec{\mu}|}$ and $\overline{\Delta\alpha}$ correspond to the difference dipole moment and polarizability, respectively, between the ground and excited state for the transition at 346 nm (TMpCA-n) and 372 nm (TM7HC-n). $\overline{|\Delta\vec{\mu}|}$ includes an enhancement due to the cavity field, f_c, and $\overline{\Delta\alpha}$ to f_c^2 (see Materials and Methods). The ratio $|\hat{m}\cdot\Delta\vec{\mu}|/|\Delta\vec{\mu}|$ is the cosine of the angle between the difference dipole moment, $|\Delta\vec{\mu}|$, and the unit vector in the direction of the transition dipole moment, $\hat{m}$. $\Delta\alpha_m$ corresponds to the change in polarizability along the transition dipole vector and is reported in Å^3.

Electronic-Structure Calculations. *Geometry Optimization.* The geometries of the protonated and anionic species were optimized using density functional theory (DFT) as implemented in the Amsterdam density functional (ADF) package.[32] The BLYP generalized gradient approximations (GGA) for the exchange and correlation functional, which combines Becke's GGA[33] for the exchange with the Lee, Yang, and Parr GGA correlation functional,[34] were used in the DFT calculations. The calculations were done with a triple-ζ Slater-type orbital (STO) basis set with a single set of polarization functions. In addition to the chromophores that have been studied here (Scheme 1a−d), we have also calculated the electronic properties of a system that is modeled in an environment similar to that found in the protein, the model-pG system, in which the hydrogen-bonded residues are included (Scheme 1e). The starting geometry for the model-pG system, taken from the PDB database,[35] was re-optimized with the constraint that the carbon atoms at the

TABLE 3: Electronic Transition Energies[a] of TMpCA-n and TM7HC-n

solvent (ϵ_0)	TMpCA-n $\tilde{\nu}_{max}$ (λ_{max})	$_{\Delta}\tilde{\nu}$ expt	TM7HC-n $\tilde{\nu}_{max}$ (λ_{max})	$_{\Delta}\tilde{\nu}$ expt
THF (2)	30580 (327)	0	27620 (362)	0
(i) MeTHF (5)	30300 (330)	−280	27550 (363)	−70
(ii) MeTHF (19)	28900 (346)	−1680	26880 (372)	−740
methanol (33)	30300 (330)	−280	23585 (424)	−4040
tris buffer (80)	30210 (331)	−370		
Gly/tris buffer	30300 (330)	−280		
1st transition (TDDFT)	27027 (370) ($S_0 \rightarrow S_2$)	−3553	26945 (371) ($S_0 \rightarrow S_3$)	−675
2nd transition (TDDFT)	29499 (339) ($S_0 \rightarrow S_3$)	−1081	29155 (343)($S_0 \rightarrow S_5$)	+1535

[a] The transition energies, $\tilde{\nu}_{max}$, of the neutral molecules, TMpCA-n and TM7HC-n, are reported in wavenumbers (cm^{-1}) and in nanometers in parentheses (λ_{max}) in tetrahydrofuran (THF), methyl tetrahydrofuran (MeTHF) (i), methanol, Tris buffer at pH7, and 55/45 (v/v) solution of glycerol and Tris buffer at room temperature and in MeTHF at 77 K (ii). The static dielectric constant, ϵ_0, for these solvents are reported in parentheses. The two lowest allowed transitions from TDDFT calculations are also reported: $S_0 \rightarrow S_2$ and $S_0 \rightarrow S_3$ for TMpCA-n, and $S_0 \rightarrow S_3$ and $S_0 \rightarrow S_5$ for TM7HC-n.

terminal methyl groups are fixed. The resulting geometry compares well to the most recent X-ray structure.[36]

Electronic Properties. The electronic transitions energies for the first strongly allowed transitions of the anions and the neutral molecules estimated from the TDDFT calculations are reported in Tables 1 and 3, respectively. The molecular orbitals that primarily contribute to the electronic transitions that are in best agreement with experiment are also presented here for TMpCA-a. The atomic charge densities, derived from the electrostatic potential (ESP) and the dipole moments in the ground state, μ_{gs},[37] were obtained from the DFT calculation, and the ESP charges and the excited-state dipole moments, μ_{es}, of the first allowed singlet excited state were obtained from the recently developed DFT-based restricted open-shell Kohn−Sham (ROKS)[38] method as implemented in the Car-Parrinello molecular dynamics (CPMD) code.[39] The electronic excitation in ROKS is modeled by transferring a single electron to an unoccupied orbital, thus assuming a HOMO−LUMO single excitation. The electron correlation is included through the exchange-correlation potential rather than by using many determinants, as in wavefunction based ab initio approaches.

The ROKS method, which is used to calculate μ_e and the atomic charge distributions, is applicable for a transition that is primarily of HOMO to LUMO character and would be unreliable when promotions from HOMO−n or to LUMO+n levels must be taken into account. The latter is the case for the transitions with large oscillator strengths in TMpCA-n and TM7HC-n. Therefore, we have used configuration interaction with single excitations (CIS) calculations, within the Gaussian 98 package,[40] where the additional transitions are included for estimating the excited-state dipole moments and charge distributions. The Mulliken atomic charges in the ground and excited states from the CIS calculations and μ_{gs}, μ_{es}, and the ground-state polarizability, α_{gs}, were determined from self-consistent field (SCF) calculations using the 6-31G(d,p) basis set. The excited-state polarizability, α_{es}, was determined from the finite-field method (see ref 30 for the application). The values of μ_{gs} and μ_{es} calculated for the anions from CIS are also reported (Table 1), although the corresponding electronic transition energies are overestimated by >10 000 cm^{-1} in these systems.

For the reasons given above, we have chosen to present the evaluation of the atomic charge densities and electrostatic properties for the anions from the DFT/ROKS method and for the neutral molecules from the CIS calculations. However, additional calculations on the anions and the neutral molecules show that the results from the two different methods are rather similar both for the ground- and excited-state properties. Moreover, the *trends* of the atomic charge differences from both ESP and Mulliken charges are also similar, although the absolute values of the partial atomic charges differ.[25] Here, the charge shifts will only be interpreted qualitatively to determine the direction of charge displacement. Even better understanding of the impact of charge transfer is garnered from the analysis of the molecular orbitals involved in the electronic excitation (specifically the HOMO and LUMO) and provides useful insight into the photoreactivity of the excited-state species.

Comparison to Experiment. The gas-phase values of $\overline{\Delta\alpha}$ and $\Delta\mu$, estimated from these calculations, have been solvent corrected to compare them directly to condensed-phase results. The reaction-field corrections are applied for a point dipole in the center of an (prolate) ellipsoidal cavity with semi-axes of length, 6.5 × 2.5 × 2.5 Å. In addition, including an enhancement due to the cavity field, f_c, which, if could be evaluated experimentally, would have concomitantly diminished the magnitudes of $\overline{\Delta\alpha}$ and $|\Delta\vec{\mu}|$ reported in Tables 1 and 2. Instead the gas-phase values are scaled by f_c.[29] A more detailed explanation and the application of these corrections to the gas-phase values may be obtained in refs 41 and 17. The (calculated) gas-phase values are labeled with the superscript "gas", whereas ground- and excited-state properties are appended with the subscript, "gs" or "es", respectively. Solvent corrected gas-phase values do not include the superscript gas.

Results

Experimental Electronic Properties of Anions: TMpCA-a and TM7HC-a. In Figure 1, the absorption spectra of TMpCA-a (part a) and TM7HC-a (part b) are shown in the CAPS buffer solution at pH 10 (light dashed line), in the glycerol-buffer solution at room temperature (light solid line), and in the corresponding glycerol-buffer glass at 77 K (dark solid line). The latter is the environment in which the Stark spectra are obtained. Also included for comparison are the absorption spectra of the proteins containing the corresponding deprotonated cofactors (light dotted line), WT-PYP in Figure 1a and L-PYP in Figure 1b (see Table 1 for absorption maxima). The electronic transition energies of the model chromophores are not only higher than in the protein but the spectra are much broader as well. The absorption maximum of TMpCA-a (λ_{max} = 384 nm) is ≈3550 cm^{-1} higher in energy than in the protein (λ_{max} = 446 nm), and the full width at half-maximum (fwhm) of ≈5000 cm^{-1} is nearly twice that of WT-PYP. These differences are less pronounced in TM7HC-a, where the electronic transition energy (λ_{max} = 421 nm) is ≈1200 cm^{-1} higher than in the protein (λ_{max} = 444 nm) and the fwhm only 800 cm^{-1} greater than in L-PYP (≈2200 cm^{-1}). On the addition of glycerol, the absorption maxima of TMpCA-a and TM7HC-a red shift by 290 and 160 cm^{-1}, respectively, and then blue shift by 680 and 280 cm^{-1}, respectively, when the temperature is

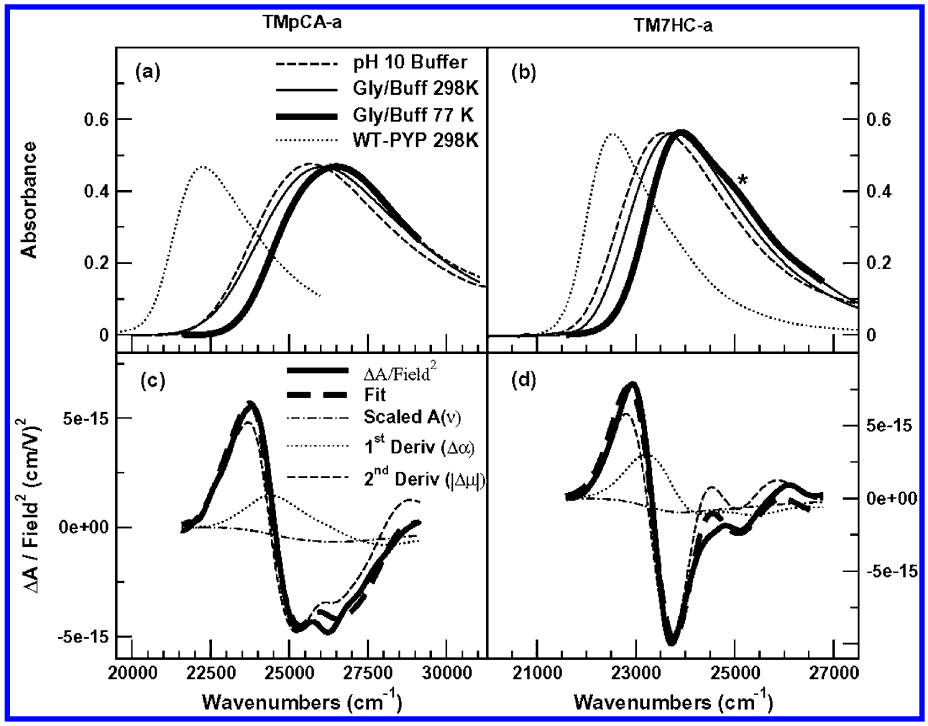

Figure 1. Absorption spectra of the anions are shown in (a) TMpCA-a and (b) TM7HC-a, in 40 mM CAPS buffer (pH 10) at 298 K (light dashed line), in glycerol-buffer (55/45 v/v) solution at 298 K (light solid line) and in the glycerol-buffer glass at 77 K (dark solid line). The absorption spectra of WT-PYP in (a) and L-PYP in (b) are shown in light dotted lines. Field-normalized Stark spectra (dark solid lines), fits (dark dashed lines), scaled absorption (light dot−dash lines), first- (light dotted lines) and second- (light dashed lines) derivative components of the fits to the Stark spectra (see eq 1) are shown in (c) for TMpCA-a and in (d) for TM7HC-a.

lowered to form a glass. Note that, in contrast to TMpCA-a, the absorption spectrum of TM7HC-a in the glycerol-buffer glass shows some vibronic structure at 77 K (marked with a star in Figure 1b). Overall, the shift of the absorption maxima of TMpCA-a and TM7HC-a follow a similar trend to that of the cofactors in the protein environment,[9] upon the addition of glycerol and upon glass formation, albeit much larger in magnitude.

The Stark spectra of TMpCA-a (Figure 1c) and TM7HC-a (Figure 1d), corresponding to the absorption spectra in the glycerol-buffer glasses, are shown in the dark solid lines. They have been normalized to the square of the applied electric field (see eq 1) and are then fit to the (wavenumber-normalized) derivatives of the corresponding absorption spectra. The LLSQ fits (dark dashed line) to the derivatives of the absorption lineshapes for both TMpCA-a (Figure 1c) and TM7HC-a (Figure 1d) reproduce the magnitudes and shapes of the Stark signals in the main region of absorption quite well. The scaled absorption function and the scaled derivatives are the first (light dot−dashed), second (light dotted), and third (light dashed) terms, in eq 1, the sum of which comprises the fit to the Stark spectrum. The average change in polarizability, $\overline{\Delta\alpha}$, and the magnitude of the change in dipole moment, $|\Delta\vec{\mu}|$, obtained from the coefficients of the first- and second-derivatives components of the fits, $b_{54.7}$ and $c_{54.7}$, respectively, are reported in Table 1. In the anions, the $|\Delta\vec{\mu}|$'s of 26 D in TMpCA-a and 15 D in TM7HC-a are very similar to that measured for the corresponding cofactors in the protein environment.[9] Moreover, these large values of $|\Delta\vec{\mu}|$ comprise the primary contribution to the field-dependent changes in the absorption (compare light and dark dashed lines in Figure 1, parts c and d). A much smaller contribution to the overall Stark signal originates from the first-derivative components (light dotted lines). The $\overline{\Delta\alpha}$ value of 450 Å^3 for TMpCA-a is a factor of 2 smaller than in WT-PYP (1000 Å^3), and the $\overline{\Delta\alpha}$ value of 250 Å^3 in TM7HC-a is somewhat larger than in L-PYP (150 Å^3).

We find that the fits to the Stark spectra of both TMpCA-a (Figure 1c) and TM7HC-a (Figure 1d) are somewhat poor on the higher energy (blue) side of the main absorption bands, indicating that the electronic properties underlying this part of the absorption band differ from that of the rest of the band at lower energy. In such cases, the fit can be improved by modeling the transitions underlying the absorption to multiple gaussians. Subsequently, the Stark spectrum is fit to the derivatives of each separate band[42] to yield the electronic properties of each underlying transition. Such a fit would be based on the assumption that the gaussians used to model the absorption spectrum accurately represent the separate transitions. However, due to the broad and relatively un-structured nature of the absorption bands, it was not possible to uniquely deconvolve the absorption spectrum and obtain a reliable estimate for the electronic properties for a blue-absorbing state or species. Therefore, because it was possible to obtain quite a good fit to the electroabsorption signal from the derivatives of the absorption line shape, and lacking any additional experimental evidence to position the gaussians, we did not attempt to uniquely extract the electro-optical parameters in these regions (Figure 1: TMpCA-a > 25 500 cm^{-1} and TM7HC-a > 24 000 cm^{-1}). The values of $|\Delta\vec{\mu}|$ and $\overline{\Delta\alpha}$ extracted from such a good fit to the absorption lineshape provide a relatively reliable estimation for the change in electronic properties of TMpCA-a and TM7HC-a in the main absorbance regions (Table 1).

Experimental Electronic Properties of Neutral Molecules: TMpCA-n and TM7HC-n. In Figure 2, the absorption spectra of TMpCA-n (part a) and TM7HC-n (part b) are shown in MeTHF at room temperature (dashed line) and in the glass at 77 K (solid line). The absorption maxima red shift when the temperature is lowered to 77 K. The change in the dielectric

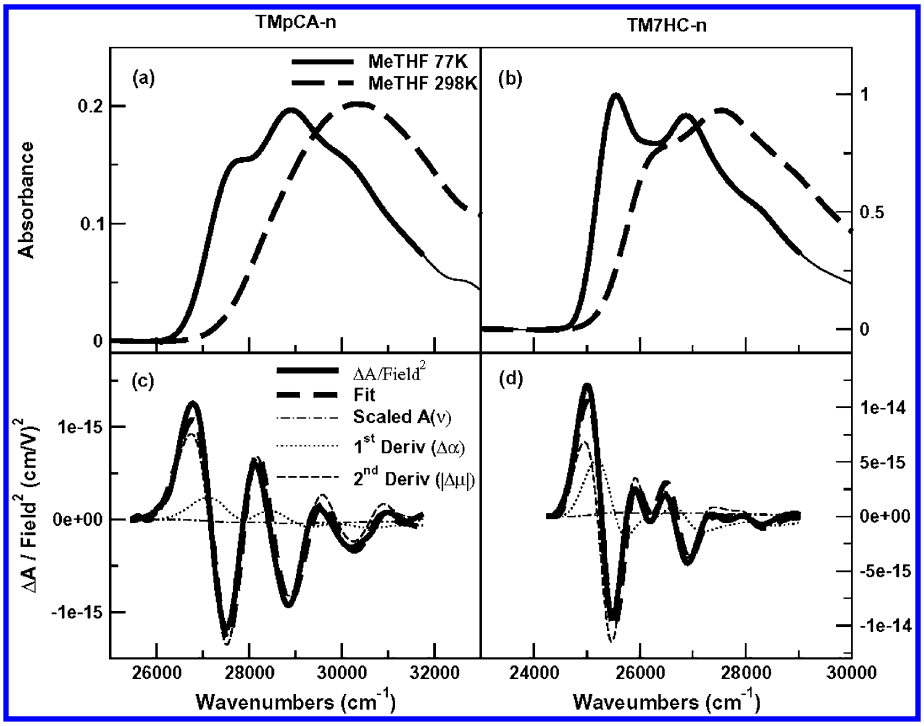

Figure 2. Absorption spectra of (a) TMpCA-n and (b) TM7HC-n are shown in MeTHF at room temperature (dashed line) and at 77 K in MeTHF glass (solid lines). Field-normalized Stark spectra (dark solid line), fits (dark dashed line), scaled absorption (light dot−dash lines), first- (light dotted lines) and second- (light dashed lines) derivative components of the fits to the Stark spectra (see eq 1) are shown in (c) for TMpCA-n and in (d) for TM7HC-n.

properties of MeTHF upon glass formation, particularly ϵ_0 from 5 to 19,[43] is much larger than in the glycerol-buffer solution. This change not only produces larger shifts in the electronic transition energies of both TMpCA-n and TM7HC-n upon lowering the temperature but also produces shifts in the opposite direction, to lower energy (Table 3). Note that, for TMpCA-n, the absorption spectrum sharpens, in contrast to TMpCA-a in the glycerol-buffer glass, and a shoulder is apparent at 362 nm (≈27 620 cm^{-1} in Figure 2a). This is also evident in TM7HC-n, where the red shifted shoulder at ≈25 500 cm^{-1} at low temperature, presumably the 0−0 transition, is not only more resolved but also increases in intensity relative to the absorption maximum. The feature is present independent of solute concentration and is not due to aggregation. In addition, on lowering the temperature, it appears that the ground and/or excited states of TMpCA-n is stabilized to a greater extent than TM7HC-n, as evident in the twofold larger shift of its absorption maximum (330−346 nm: ≈1400 cm^{-1} vs 363−372 nm: ≈660 cm^{-1}).

The corresponding Stark spectra (dark solid lines) and fits (dark dashed lines) in the MeTHF glass for TMpCA-n (Figure 2c) and TM7HC-n (Figure 2d) are also shown. The same legend key has been used as in Figure 1. The scaled absorption function (light dot dashed), and the first (light dotted) and second (light dashed) derivatives of the absorption spectra are a measure of the relative contributions of the corresponding electrostatic properties to the total Stark signal. The electro-absorption spectra of both TMpCA-n and TM7HC-n are highly structured, consistent with the distinct vibronic structure apparent in the absorption spectra at 77 K. In contrast to the anionic systems, the fits we obtain to the Stark spectra are very good across the entire absorption lineshape indicating that the electronic properties are uniform across the absorption band. Even the fit to the Stark spectrum of TM7HC-n, although it exhibits an unusual increase in the intensity of the 0−0 transition at 77 K (≈25 500 cm^{-1}), is quite good. The corresponding electro-optical parameters obtained from the fits to the absorption lineshape are reported in Table 2 for the neutral molecules. The $|\Delta\vec{\mu}|$ values for TMpCA-n (9.0 D) and TM7HC-n (6.1 D) are nearly three times smaller than in the corresponding anionic species (see Table 1). However, the major components of the Stark signals of both TMpCA-n and TM7HC-n are due to contributions from $|\Delta\vec{\mu}|$, with only much smaller contributions from $\overline{\Delta\alpha}$ (see differences between the second-derivative components and the fits in Figure 2, parts c and d), which is 62 $Å^3$ for TMpCA-n and is 120 $Å^3$ for TM7HC-n (Table 2). The Stark spectra with χ set at 90°, which were also measured in the MeTHF glass, are not shown here (they have the same shape and features as the spectra obtained at 54.7° except that they are smaller in magnitude). From these data, we find that the change in dipole moment, $|\Delta\vec{\mu}|$, is nearly parallel to the transition dipole moment, $\hat{m}$, in TM7HC-n ($|\hat{m}\cdot\Delta\vec{\mu}| \cong |\Delta\vec{\mu}|$), whereas the angle between $|\Delta\vec{\mu}|$ and the transition dipole moment is nearly 30° for TMpCA-n (Table 2). The change in polarizability along the transition moment, $\Delta\alpha_m$, for both TMpCA-n and TM7HC-n are approximately a factor of three larger than $\overline{\Delta\alpha}$.

Ab Initio Calculations. *Transition Energies*. TDDFT calculations on TMpCA-a and TM7HC-a show that the first excitation energies with considerable oscillator strengths ($S_0 \rightarrow S_2$) can be described in terms of a HOMO to LUMO promotion accounting for 90% and 80% of the excitation, respectively. The transition is at 402 nm (24 881 cm^{-1}) for TMpCA-a and at lower energy (410 nm, 24 360 cm^{-1}) for TM7HC-a (Table 1) with oscillator strengths, f_{osc}, of 0.95 and 0.43, respectively. The calculated values are merely 1000 cm^{-1} lower in energy and 600 cm^{-1} higher in energy than in the pH 10 buffer solutions of TMpCA-a and TM7HC-a, respectively. The TDDFT calculated electronic transition energies for the neutral chromophores are more complex than for the anionic molecules; there are two close lying transitions with medium oscillator strengths for both TMpCA-n and TM7HC-n (Table 3).

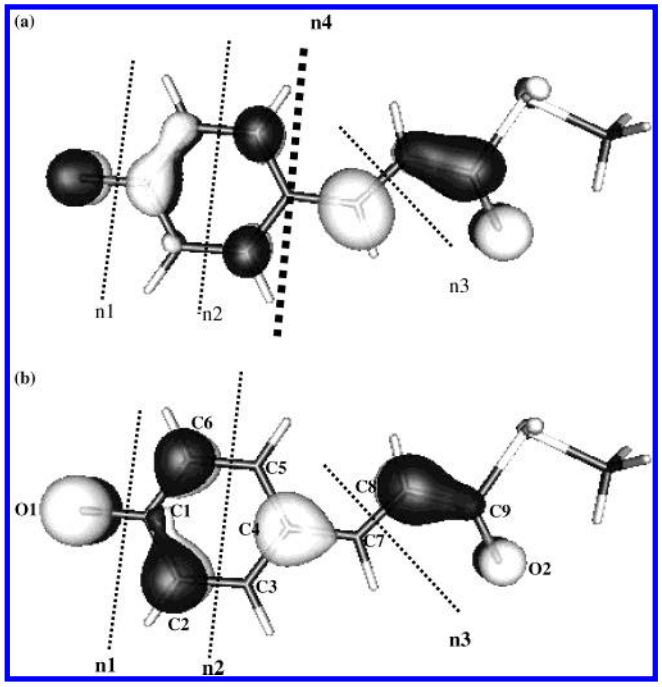

Figure 3. Molecular orbitals of TMpCA-a: (a) LUMO and (b) HOMO. The dark and light regions represent the positive and negative parts of the wave function, respectively. The broken lines correspond to the nodes in the wave functions: n1, n2, and n3 in the HOMO and additionally n4 in the LUMO.

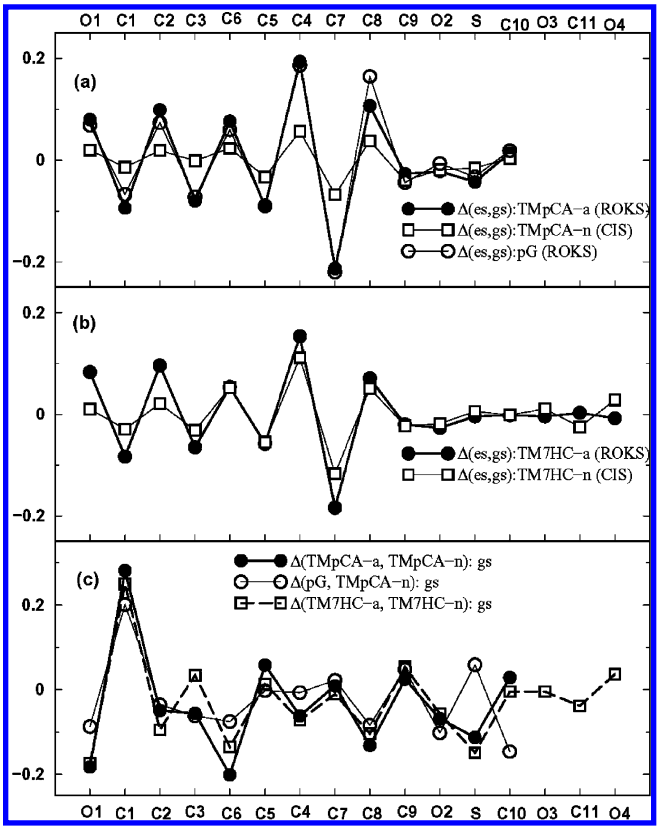

Figure 4. ESP (DFT/ROKS) and Mulliken (CIS) atomic charge differences between the ground and excited states are shown in (a) for TMpCA-a (solid circles), TMpCA-n (open squares), and model-pG (open circles) and in (b) for TM7HC-a (solid circles) and TM7HC-n (open squares). In (c), the ground-state (gs) ESP charge differences between TMpCA-a and TMpCA-n (solid circles), between model-pG and TMpCA-n (open circles), and between TM7HC-a and TM7HC-n (open squares) are shown. Atoms O3, C11, and O4 are only present in TM7HC-a and TM7HC-n (parts b and c).

In the ground state of TMpCA-a, there are three nodes in the wavefunction in the part of the HOMO most affected by the promotion of an electron to the LUMO (see Figure 3): n1, between O1 and C1, n2, between the C5−C6 and C2−C3 bonds, and n3, between C7 and C8. The wavefunction over C3, C4, C5, and C7 is of the same sign with the electron density localized at C4 and changes sign between C7 and C8. In the LUMO of TMpCA-a, besides a decrease in electron density on O1, the most marked change occurs in the C3−C4−C5−C7 region with the formation of a new node at C4 (see n4 in Figure 3b). The node between C7 and C8 in the HOMO (n3 in Figure 3a) is also present in the LUMO (Figure 3b) but with the electron density now localized on C7. Therefore, a change in the sign of the wavefunction, an antibonding break, is produced closer to the middle of the C7−C8 bond and increases the local antibonding character. These changes will be discussed in the context of charge displacement and the subsequent consequences on the photoreactivity of the molecule. The HOMO and LUMO of TM7HC-a (see Figure S1 in the Supporting Information) are similar to TMpCA-a, except that the wavefunction on O3 and O4, of the same sign as on C3−C4−C5−C7, extends the π-conjugated system over this region.

For TMpCA-n $S_0 \rightarrow S_2$ and $S_0 \rightarrow S_3$ at 370 nm ($f_{osc} \approx 0.40$) and 338 nm ($f_{osc} \approx 0.34$), respectively, are allowed. Both transitions consist of HOMO−LUMO (62% for $S_0 \rightarrow S_2$ and 28% for $S_0 \rightarrow S_3$) and HOMO-1 to LUMO (21% for $S_0 \rightarrow S_2$ and 58% for $S_0 \rightarrow S_3$) promotions. For TM7HC-n, we find that the first allowed transition is $S_0 \rightarrow S_3$ ($f_{osc} \approx 0.15$) at 371 nm (26 940 cm^{-1}), whereas $S_0 \rightarrow S_5$ at 343 nm (29195 cm^{-1}) is about twice as intense ($f_{osc} \approx 0.26$). Both of these transitions contain promotions from HOMO-2 to LUMO (55% for $S_0 \rightarrow S_3$ and 21% for $S_0 \rightarrow S_5$) and HOMO-3 to LUMO (31% for $S_0 \rightarrow S_3$ and 60% for $S_0 \rightarrow S_5$). The first allowed transitions in both TMpCA-n and TM7HC-n are much lower in energy than the experimental values, whereas the second lowest (allowed) transitions compare quite well to the experimental values. These transitions, $S_0 \rightarrow S_3$ for TMpCA-n and $S_0 \rightarrow S_5$ for TM7HC-n, are underestimated by ≈700 cm^{-1} (TMpCA-n) and 1600 cm^{-1} (TM7HC-n) with respect to the condensed phase (Table 3). We note that, in all four systems, none of the (first ten) transitions generated in our calculations with a considerable oscillator strength are of n−π* character, which has been previously identified in pCA both experimentally[14] and in calculations.[20] It is possible that a different molecular geometry, away from the global energy minimum, can produce such a transition in TMpCA as well.

Charge Density Distributions. The charge differences between the ground state and the excited state in the Franck−Condon region, from ESP (circles) and Mulliken charge analysis (squares), are shown for the anions and the neutral molecules in Figures 4a (TMpCA and model-pG) and Figure 4b (TM7HC). The charge differences estimated for TMpCA (Figure 4a) indicate that, on excitation, the anion (solid circles) exhibits significantly larger changes in electronic charge on atoms O1 through C8, than in TMpCA-n (open or solid squares). The phenolate oxygen, O1, in TMpCA-a is significantly more electropositive in the excited state due to charge shift *away from* O1, while the main electron acceptor is C7. The charge differences alternate within the phenol ring and the carbon backbone, with the most pronounced changes manifested on C4, C7, and C8, in TMpCA-a. This pattern in the charge difference, between the ground and excited state, is also mirrored in the extended model-pG system[44] (compare solid and open

circles in Figure 4a), despite the differences in the ground-state charge distribution (Figure 4c).

There is a similar alternation in charge density in the phenol ring and along the carbon backbone in TM7HC, with the largest changes manifested on C4 and C7 in the excited state. Furthermore, as in TMpCA-a, it is O1 that is intimately linked to the charge-transfer process of TM7HC-a and not in TM7HC-n. The charge differences between TM7HC-a and TM7HC-n (Figure 4b) are, however, much more similar than that between TMpCA-a and TMpCA-n. In Figure 4c, we have plotted the differences in the ground-state charges between the neutral molecules and the corresponding anions, as well as between the model-pG system and TMpCA-n. For consistency, and since DFT calculations are considered to be quite reliable in the ground state, these charge differences are estimated from ESP charges. The ground-state charge difference between TMpCA-a and TM7HC-a and the corresponding neutral conjugates are very similar, whereas that between model-pG and TMpCA-n (Figure 4c, open circles) deviates somewhat from this pattern on sulphur and C10. In addition, the increase in negative charge on the phenolate oxygen, O1, in TMpCA-a (and in TM7HC-a) compared to TMpCA-n (and TM7HC-n) is twice as much as on model-pG, in the ground state.

Dipole Moments and Polarizabilites. Values of μ_{gs}^{gas} estimated for TMpCA-a and TM7HC-a from DFT and CIS calculations, on the order of 7−9 D (Table 1), are much larger than in the corresponding neutral molecules (Table 2). In TMpCA-n, the value of μ_{gs}^{gas} is ≈3 D, both from DFT and CIS and nearly half that of TM7HC-n (≈6 D). The $\Delta\mu^{gas}$ estimated from DFT/ROKS calculations for the anions are on the order of 3 D and indeed even smaller from the CIS calculations (Table 1). In contrast, the $\Delta\mu^{gas}$'s for TMpCA-n (2.9 D) and TM7HC-n (1.9 D), are in much better agreement with experiment. The difference polarizability evaluated from α_{gs}^{gas} and α_{es}^{gas} (Table 2) is more than an order of magnitude smaller than experiment for TM7HC-n and a factor of six smaller for TMpCA-n. For the anions, solvent correcting the $\Delta\mu^{gas}$ values enhances them by a factor of two, which nevertheless are much smaller than the experimental results. On the other hand, accounting for solvation, enhances the $\Delta\mu^{gas}$ values for the neutral molecules by 25 to 30%, bringing theory and experiment into much better agreement (Table 2).

Discussion

Electronic Properties of Anionic Chromophores. *Experimental Electrostatic Properties.* One of the most important findings in this work is that the 25 D change in dipole moment of TMpCA-a is remarkably similar to that measured in WT-PYP (26 D). Except for the methyl group that replaces the covalent linkage to the cysteine group in the protein, TMpCA-a and the cofactor of WT-PYP are structurally identical. Therefore, a similar pattern of charge transfer is exhibited in this chromophore, both in the protein environment and in solution; that is, $|\Delta\vec{\mu}|$ is indeed an intrinsic property of the chromophore and is not significantly enhanced or diminished due to the surrounding protein environment. Furthermore, the similarity in $|\Delta\vec{\mu}|$ for TM7HC-a (15 D) and L-PYP (13 D) also supports this inference. The value of $|\Delta\vec{\mu}|$ for TMpCA-a implies that one electron moves over 5 Å, or alternatively, a partial electronic charge moves over a longer distance (one electron separated by 1 Å corresponds to 4.8 D in vacuo). In TMpCA-a, this charge shift is most likely to occur from the electron rich phenolate oxygen, O1, on which negative charge is presumed to be localized in the ground state, toward the electrophilic carbon double bond ≈5 Å away. The partial atomic charge differences calculated here for the anions support this assignment; the largest difference in charge density is evidently manifested on O1 and C7 (Figure 4a). Furthermore, despite decreasing the flexibility of TMpCA by the insertion of a ring, the calculated charge shift in TM7HC-a is similar to that in TMpCA-a, from O1 toward C7, albeit of smaller magnitude (Figure 4b).

Although there is a striking similarity in the values of $|\Delta\vec{\mu}|$ for the two model chromophores and the cofactors in the protein, there are differences in the changes in polarizability between the two environments. The $\overline{\Delta\alpha}$ measured in WT-PYP (≈1000 Å^3) is a factor of two larger than TMpCA-a (450 Å^3), presumably because the LUMO in the excited state is extended beyond the cofactor and over the adjacent arginine residue in the protein.[18,19,21] Consequently, α_{es} would be much larger than α_{gs}. However, we cannot readily explain why $\overline{\Delta\alpha}$ in TM7HC-a (250 Å^3) is larger than in L-PYP (150 Å^3). Considering that the Stark spectra of the anions and the cofactor in the protein environment[9] are quite similar to the second-derivative components, the first-derivative components, arising from $\overline{\Delta\alpha}$, are only minor contributors to the overall Stark signals and therefore less accurately determined. A factor of two increase or decrease in the magnitude of this component would not drastically affect the fit quality.

Origin and Impact of Charge Motion in TMpCA-a and TM7HC-a. The simplest model for charge shift in TMpCA, to understand the impact of charge transfer in the protein environment, would be to use a valence-bond scheme.[7,9] However, such valence bond representations are resonance structures that provide an idea for the average charge distribution in the ground state. They do not reflect the charge distribution of the excited state or the consequence of the dipole moment change. Indeed, based on the bond lengths of PYP (dark) from X-ray crystal data,[36] dark-pG was suggested to stabilize the negative charge on the molecule by adopting a hybrid in the ground state between a phenolic and quinonic structure, with the negative charge localized either on O1 or on O2, respectively.[36] Nevertheless, the bond lengths in the phenyl ring, and of the O1−C1 and C9−O2 bonds, in the optimized structures of TMpCA-a and model-pG (see Table S1 in Supporting Information), and even the X-ray structure,[36] suggest that these systems are quinone-like, with the negative charge localized on O1. In contrast, TMpCA-n is more phenol like. On excitation, the charge, which is localized on O1 in the ground state, is transferred to C7 in the excited state (Figure 4, parts a and b), which consequently increases the flexibility of the molecule. This charge displacement pattern is also seen in model-pCA compounds.[18,21]

On excitation, the additional node produced in the electron density of the LUMO (n4 in Figure 3) "disconnects" the phenyl ring from C7 and makes it more flexible in the excited state than in the ground state, where the C3−C4−C5−C7 system is "locked" in place. Moreover, the node of the wave function is now centered between C7 and C8 in the LUMO, which was somewhat displaced toward C7 in the HOMO. Consequently, there is now a distinct antibonding break between C7 and C8 in the LUMO and the bond is expected to twist more easily in the excited state. Furthermore, the higher the energy of the antibonding orbital, the smaller is the gap between the excited-state species and the activation barrier for isomerization.

These effects in the LUMO can be related to increasing single-bond character of the different bonds. Indeed, preliminary geometry optimization calculations in the excited state, using the ROKS method, primarily shows a considerable elongation

of the C7−C8 bond. The disappearance of the C═C stretch observed in a recent ultrafast mid-IR study[5] is consistent with the increase in the single bond character of the C7−C8 bond. The fact that the cofactor in PYP, similar to TMpCA-a, in a trans configuration in the ground state adopts a distorted configuration immediately within 200 fs can be explained by the changes in the orbital symmetry induced by the charge displacement from O1 to C7 on photon absorption. The additional observations of an upshift in the C═O stretching frequency of Glu46, indicative of the weakening of the hydrogen bond between O1 and Glu46, would be initiated by a loss of negative charge on O1. The concomitant downshift of the bands associated with the stretches of the phenolate ring coupled to O1 may be explained by the increasing antibonding character of the orbitals localized on the phenyl ring in the LUMO.

Gas-Phase Dipole Moments. The $\Delta\mu^{gas}$ values of 2−3 D (Table 1) evaluated for the anions, both from CIS and DFT/ROKS, are in poor agreement with the experimental values which are a factor of ten larger. In addition, presuming that there is an increase in the polarity of the (solvent) environment and/or greater interaction between the solute and solvent due to electrostriction, the blue shift of the absorption maximum at 77 K would suggest that $\Delta\mu < 0$ in both TMpCA-a and TM7HC-a. In fact, the ROKS/DFT calculations show that $\mu_{gs}^{gas} > \mu_{es}^{gas}$ for both anions (Table 1). The discrepancy between the magnitudes of the experimental and calculated values may arise if either the charge-transfer distance or the magnitude of the charge that is transferred is underestimated. Even if the maximum charge-transfer distance, for the same charge, was to be from one end to the other end of the molecule, it would at most increase the values of $\Delta\mu^{gas}$ by a factor of two; therefore, either μ_{gs}^{gas} and/or μ_{es}^{gas} are (significantly) underestimated. If indeed $|\Delta\vec{\mu}|$ is negative, μ_{gs}^{gas} is then too small to account for $|\Delta\vec{\mu}|$'s of 25 or 15 D. In general, electronic-structure calculations are considered to provide a reliable estimate for ground-state dipolar properties. However, such an evaluation for the estimation of these properties in anions is not readily available in the literature, and the finding here suggests that theoretical modeling of such anionic systems, even in the ground state, needs to be checked. Alternatively, if $|\Delta\vec{\mu}|$ is positive, then μ_{es}^{gas} is underestimated. In either case, larger μ_{gs}^{gas} or μ_{es}^{gas} would be produced if the negative charge were to be strongly localized at one end of the molecule, and it is the de-localization of the negative charge that appears to be overestimated. For example, the loss of a proton increases the effective charge on O1 by only 40% to 50% in the anions in the ground state (solid circles in Figure 4c). Further theoretical investigations are needed to elucidate the origin of this discrepancy in the dipole moments.

One suggestion is obtained from the examination of the HOMO-1 orbital, which houses the lone pair on O1. The electronic charge is strongly localized on O1, and the orbitals on O1 and C1 are strongly antibonding. Presumably, a promotion from such a HOMO-1 to the LUMO could produce a large change in dipole moment. However, this promotion does not contribute significantly to any allowed transition. Such a HOMO-1 to LUMO transition would be an n−π* type transition.[14,20] Although n−π* transitions are typically lower in energy than π−π* transitions, in this case, a higher energy transition would actually bring theory and experiment into even better agreement. When calculating the electronic eigenvalues in the presence of an external field, one to two orders of magnitude larger than the fields applied in the Stark experiment, the energy gap between the HOMO and HOMO-1 gets smaller and gives rise to an electronic excitation with contributions coming both from HOMO and HOMO-1 to LUMO transitions.

Environmental Effects on the Electronic Properties of TMpCA-a. The similarity in the values of $|\Delta\vec{\mu}|$ between TMpCA-a and WT-PYP and between TM7HC-a and L-PYP indicate that the electrostatic interactions between the amino acid residues and the cofactor in the protein are just as strong as in the glycerol-buffer glass and the model chromophores. Within dielectric continuum theory, presuming that the static dielectric of the glycerol−buffer environment is approximately a factor of 10 larger (ϵ_0(water) ≈ 80) than in the protein,[45] a much stronger reaction field would be expected. Consequently, the dipole moments of TMpCA-a and TM7HC-a in solution should be larger than in the protein. Nevertheless, calculations indicate that the molecular orbitals, HOMO and LUMO, and the charge shift pattern in the model-pG system are nearly the same as in TMpCA-a (compare solid lines with open and closed circles in Figure 4a). Therefore, the flipping of the thio-ester moiety should be facilitated to a similar extent in the excited state by reducing the activation barrier to trans−cis isomerization.[9,19] Indeed, it is so easy to overcome this barrier in the protein that (bathochromic) photoproducts with distorted/twisted geometries were generated in WT-PYP, even at 77 K.[9,46] However, no such photoproducts appear to be generated on excitation of TMpCA-a in the experiments performed here.

Although the similar $|\Delta\vec{\mu}|$'s of TMpCA-a and WT-PYP would imply that it should be just as easy to overcome the twisting barrier for TMpCA-a, this appears not to be the case for the isolated chromophores in solution. Perhaps, this is because the chromophore, which is in direct contact with the glycerol and water molecules, is not "protected" within the protein pocket as it is in WT-PYP. Although both molecules interact with their environments quite strongly by forming hydrogen bonds, the nature of the hydrogen bonding is much more specific in the protein pocket: Glutamine 46 hydrogen bonds to the phenolate oxygen, O1, and the cysteine residue to the carbonyl oxygen, O2. To model such targeted interactions between the "solvent" and "solute" in the protein, modeling the solvent as a continuum would not be ideal. Therefore, it is likely that dielectric continuum theory does not provide an accurate estimate for the reaction field and the concomitant effect on the electronic properties of the chromophores.

Additionally, TMpCA-a, in contrast to pG, is free to hydrogen bond in a more random fashion. It is more likely that a much wider distribution of ground-state conformations is present, which is further aided by the flexibility of TMpCA. Indeed, this is immediately evident from the fwhm of the absorption spectrum of TMpCA-a (≈5000 cm^{-1}), which is nearly twice that of WT-PYP. The narrower absorption bandwidth indicates that a more restricted set of cofactor geometries are stabilized in the protein pocket. Furthermore, if different conformers of TMpCA-a are present in the ground state, one may presume that excitation of these different conformers may permit the anion to access different pathways toward or alternatively away, from the isomerization reaction coordinate and produce dynamics that are different from that in the protein.[12]

Restriction of the geometry will limit the number of polarity induced conformers that can be generated in solution and is evident in the absorption of TM7HC-a. Presumably, the additional ring in TM7HC-a results in a decrease in the flexibility of the chromophore, which is why its fwhm in solution is only one and a half times greater than L-PYP. Nevertheless, both model chromophores in solution are more sensitive to changes in the environment than the corresponding

cofactors in the protein pocket. This is also evident in the much more pronounced effects on the electronic transition energies on the addition of glycerol, and on glass formation, particularly in TMpCA-a (Tables 1 and 3). Neither TMpCA-a nor TM7HC-a are shielded from the effective change in the dielectric properties of the environment on glass formation, whereas the cofactors contained within the protein pocket primarily experience a change in the electrostatic interaction with the adjacent amino acid residue. Macroscopic changes in the environment outside the protein pocket do not appear to strongly perturb the electrostatic interactions within the protein pocket and the effect on the transition energies is therefore less pronounced.

Electronic Properties of Neutral Chromophores. *Experimental Electrostatic Properties.* The highly structured absorption spectra of TMpCA-n and TM7HC-n in the MeTHF glass and the lack of congestion in the absorption bands, in contrast to the anions, reflect the presence of a narrow distribution of ground-state conformers. Indeed, the high quality of the fits to the Stark spectra indicate that excitation within the absorption bands would populate a single excited state with similar electronic properties across the different vibronic levels. The resultant $|\Delta\vec{\mu}|$'s of TMpCA-n (9 D) and TM7HC-n (6 D), although similar to the change in dipole moment measured for the charge-transfer transitions of other (neutral) coumarins,[17,47] are significantly smaller than those of the corresponding anions. The charge distributions for the neutral molecules (Figure 4, parts a and b) indicate that, as in the anions, charge is transferred from O1 toward C7. This drastic diminution of the extent of charge transfer in the neutral molecules has an important implication for the cofactors in the protein. Presumably, it would not weaken the C7−C8 double bond sufficiently to promote the twisting of the molecule and could slow, or even completely block, trans−cis isomerization and effectively shut down the efficient functioning of the protein. Protonation of the cofactor in the protein would therefore not lower the activation barrier for trans−cis isomerization to the same extent in the excited state as it would, if it were de-protonated. These results on the neutral molecules underscore the importance of the protein environment in ensuring that the cofactor in the protein remains de-protonated in the ground state.

Although the $|\Delta\vec{\mu}|$ values measured here for TMpCA-n and TM7HC-n are similar to those of other molecules associated with charge-transfer transitions, the $\overline{\Delta\alpha}$ values are comparatively quite large; 120 Å^3 for TM7HC-n and 62 Å^3 for TMpCA-n. These large values $\overline{\Delta\alpha}$ could arise due to large excited-state electronic polarizabilites. In the sum-over-states expression (SOS), the polarizability of state i, $\alpha_i = \sum_f(|\langle f|\hat{m}_{fi}|i\rangle|^2)/(E_f - E_i)$, is proportional to the square of the transition moment and inversely proportional to the energy gap, $E_f - E_i$, with respect to each state, f, in the entire electronic manifold. Therefore, strong coupling with a nearby higher lying electronic state could account for large α_{es}^{gas}'s. Such a state, however, would not be strongly coupled to the ground state and therefore not be visible in the absorption spectrum. Transient absorption spectra[12] indicate that both of these molecules have strong excited-state absorptions at $\approx$ 350 nm, which, although 30 000 cm^{-1} higher in energy, could partially account for large α_{es}^{gas}'s.

In addition, the effect of hydrogen bonding on the electronic properties of the neutral molecules cannot be discounted, as for the anions. Hydrogen bonding interactions could account for the similarity in the absorption maximum of TMpCA-n in methanol to that in Tris-HCl buffer solution at pH 7 ($\epsilon_0 = 80$), at room temperature, although the latter is much more polar than methanol ($\epsilon_0 = 33$). Similarly, in TM7HC-n, the absorption maximum in methanol ($\epsilon_0 = 33$), where the chromophore is unlikely to be de-protonated, is quite similar to that in the CAPS buffer solution at pH 10 (Table 3). Moreover, the strong electronic response of both TMpCA-n and TM7HC-n in these solvent environments suggest that they would serve as reasonably good polarity probes of the solvent environment.

Comparison to Calculations. The agreement between experimental values of $|\Delta\vec{\mu}|$ and $\overline{\Delta\alpha}$ and those from CIS calculations, although reasonable, have turned out to be in much poorer agreement than for other charge-transfer molecules.[17] Even after including the effects of the reaction and cavity field, values of $\Delta\mu$ are a factor of 2 smaller than experiment. Nevertheless these calculations are in agreement with other experimental observations. We find that $\mu_{gs}^{gas} < \mu_{es}^{gas}$, consistent with the systematic lowering of the electronic transitions energies of both TMpCA-n and TM7HC-n, as the polarity of the solvent increases (Table 3). Furthermore, the magnitudes of these shifts are larger for TMpCA-n than TM7HC-n consistent with the larger $\Delta\mu$ of TMpCA-n. In addition, $\Delta\mu$ is parallel to the TM7HC-n transition moment, in agreement with experiment. However, a similar estimation of $|\hat{m}\cdot\Delta\vec{\mu}|$ (Table 2) for TMpCA-n, where both $\Delta\mu$ and $\hat{m}$ are oriented along the linear polyene-backbone axis, differs from the experimental finding that $\hat{m}$ makes an angle of about 30° with $|\Delta\vec{\mu}|$.

One reason there may be a deviation between experiment and calculations in the case of TMpCA-n could be because the molecule adopts a nonplanar conformation in the ground state, and $\Delta\mu$ would not necessarily be parallel to $\hat{m}$. However, the good fit to the Stark spectrum indicates the presence of one (dominant) conformation, and it is unlikely to be one that is in a distorted, energetically higher state. The disagreement between experiment and theory is more striking with the calculated $\overline{\Delta\alpha}$ values ($\approx$10 Å^3), which are a factor of six to ten smaller than the experimental values (Table 2). In general, $\overline{\Delta\alpha}$ is a much more difficult physical property to calculate, as coupling with electronic states in the entire electronic manifold needs to be taken into account (see SOS expression above). Although the ground state polarizability would be reasonably well estimated, because the main contribution to this value arises from coupling with the lowest allowed transition, it is more likely that the excited state polarizabilites are inaccurately determined particularly if, as we presume, coupling to higher electronic states have not been properly taken into account.

Conclusion

The similarity in the $|\Delta\vec{\mu}|$ values for anionic TMpCA and the cofactor in WT-PYP indicate that a similar magnitude of charge motion is produced as a consequence of photon absorption, both in the protein environment and in the condensed phase. This supports the suggestion that the intrinsic electrostatic properties of the chromophore provide the trigger for the PYP photocycle. However, the significant diminution of $|\Delta\vec{\mu}|$ by a factor of three in TMpCA-n underscores the importance of the protein environment in keeping the cofactor de-protonated in the ground state in order to produce charge motion large enough to facilitate the twisting of the cofactor in the excited state. A similar pattern for charge motion is also found to exist in the sterically hindered analogue, TM7HC, within and outside the protein, further supporting these proposals. We also find that TDDFT calculations are quite robust in being able to predict the electronic transition energies of anionic and neutral TMpCA and TM7HC. Additionally, the atomic charge density differences indicate that charge transfer occurs from the phenolate oxygen,

O1, primarily to C7 in the excited state. Consequently, the additional antibonding breaks in the wavefunction along the C4−C7 and C7−C8 bonds in the LUMO, would effectively increase the flexibility of the C4−C7−C8−C9 carbon backbone and facilitate twisting in the excited state. The calculated $\Delta\mu$'s, however significantly underestimate the *magnitude* of the charge transferred, particularly for the anions. Future studies should pay attention to re-producing the dipolar properties of the initially excited state to obtain an accurate (quantitative) description of the potential energy surface of such systems.

Acknowledgment. This project was supported by the Foundation for Fundamental Research on Matter of The Netherlands (FOM) and the Dutch Science Foundation (NWO) (L.L.P. and R.v.G.). L.L.P. also thanks Todd Martinez for fruitful discussions.

Supporting Information Available: Synthesis of anions nad neutral TMpCA and TM7HC, the HOMO and LUMO of TM7HC-a, and the bond lengths of the optimized structures. This material is available free of charge via the Internet at http://pubs.acs.org.

References and Notes

(1) Meyer, T. E.; Yakali, E.; Cusanovich, M.; Tollin, G. *Biochemistry* **1987**, *26*, 418.

(2) Sprenger, W. W.; Hoff, W. D.; Armitage, J. P.; Hellingwerf, K. J. *J. Bacteriol.* **1993**, *175*, 3096.

(3) Hoff, W. D.; Dux, P.; Hard, K.; Devreese, B.; Nugteren-Roodzant, I. M.; Crielaard, W.; Boelens, R.; Kaptein, R. *Biochemistry* **1994**, *33*, 13959.

(4) Ujj, L.; Devanathan, S.; Meyer, T. E.; Cusanovich, M. A.; Tollin, G.; Atkinson, G. H. *Biophys. J.* **1998**, *75*, 406.

(5) Groot, M.-L.; van Wilderen, L.; Larsen, D. S.; van der Horst, M. A.; van Stokkum, I. H. M.; Hellingwerf, K. J.; van Grondelle, R. *Biochemistry* **2003**, *42*, 10054.

(6) Changenet, P.; Zhang, H.; van der Meer, M. J.; Hellingwerf, K. J.; Glasbeek, M. *Chem. Phys. Lett.* **1998**, *282*, 276. Gensch, T.; Gradinaru, C.; van Stokkum, I. H. M.; Hellingwerf, K. J.; van Grondelle, R. *Chem. Phys. Lett.* **2002**, *356*, 347. Larsen, D. S.; Vengris, M.; van Stokkum, I. H. M.; van der Horst, M. A.; R. A., C.; Hellingwerf, K. J.; van Grondelle, R. *Chem. Phys. Lett.* **2003**, *369*, 563. Mataga, N.; Chosrowjan, H.; Taniguchi, S.; Hamada, N.; Tokunaga, F.; Imamoto, Y.; Kataoka, M. *Phys. Chem. Chem. Phys.* **2003**, *5*, 2454.

(7) Masciangioli, T.; Devanathan, S.; Cusanovich, M. A.; Tollin, G.; El-Sayed, M. A. *Photochem. Photobiol.* **2000**, *72*, 639.

(8) Mataga, H.; Chosrowjan, Y.; Shibata, Y.; Imamoto, F.; Tokunaga, N. *J. Phys. Chem. B.* **2000**, *104*, 5191. Genick, U. K.; Soltis, S. M.; Kuhn, P.; Canestrelli, I. L.; Getzoff, E. D. *Nature* **1998**, *392*, 206.

(9) Premvardhan, L. L.; van der Horst, M. A.; Hellingwerf, K. J.; van Grondelle, R. *Biophys. J.* **2003**, *84*, 3226.

(10) Mathies, R. A.; Lin, S. W.; Ames, J. B.; Pollard, W. T. *Annu. Rev. Biphys. Biochem.* **1991**, *20*, 518.

(11) Xie, A.; Kelemen, L.; Hendriks, J.; White, B. J.; Hellingwerf, K. J.; Hoff, W. D. *Biochemistry* **2001**, *40*, 1510.

(12) Larsen, D. S.; Vengris, M.; van Stokkum, I. H. M.; van der Horst, M. A.; de Weerd, F. L.; Hellingwerf, K. J.; van Grondelle, R. *Biophys.* J. **2004** in press.

(13) Changenet-Barret, P.; Plaza, P.; Martin, M. M. *Chem. Phys. Lett.* **2001**, *336*, 439.

(14) Ryan, W. L.; Gordon, D. J.; Levy, D. H. *J. Am. Chem. Soc.* **2002**, *124*, 6194.

(15) Bublitz, G. U.; Boxer, S. G. *Annu. Rev. Phys. Chem.* **1997**, *48*, 213.

(16) Beekman, L. M. P.; Steffen, M.; van Stokkum, I. H. M.; Olsen, J. D.; Hunter, C. N.; Boxer, S. G.; van Grondelle, R. *J. Phys. Chem. B* **1997**, *101*, 7284.

(17) Chowdhury, A.; Locknar, S. A.; Premvardhan, L. L.; Peteanu, L. A. *J. Phys. Chem. A* **1999**, *103*, 9614.

(18) Molina, V.; Merchán, M. *Proc. Natl. Acad. Sci.* **2001**, *98*, 4299.

(19) Sergi, A.; Gruning, M.; Ferrario, M.; Buda, F. *J. Phys. Chem. B* **2001**, *105*, 4386.

(20) Ko, C.; Levine, B.; Toniolo, A.; Manohar, L.; Olsen, S.; Werner, H.-J.; Martinez, T. J. *J. Am. Chem. Soc.* **2003**, *125*, 12710.

(21) Groenhof, G.; Lensink, M. F.; Berendsen, H. J. C.; Snijders, J. G.; Mark, A. E. *Proteins: Struct., Funct., Genet.* **2002**, *48*, 202.

(22) Unno, M.; Kamauchi, M.; Sasaki, J.; Tokunaga, F.; Yamauchi, S. *Biochemistry* **2002**, *41*, 5668.

(23) Thompson, M. J.; Bashford, D.; Noodleman, L.; Getzoff, E. D. *J. Am. Chem. Soc.* **2003**, *125*, 8186.

(24) Gross, E. K. U.; Kohn, W. *Adv. Quantum Chem.* **1990**, *21*, 255. Casida, M. E. In *Recent Developments and Applications of Modern Density Functional Theory*; Seminario, J. M., Ed.; Elsevier: Amsterdam, 1996.

(25) Jensen, F. *Introduction to Computational Chemistry*; Wiley: New York, 1996.

(26) Moylan, C. *J. Phys. Chem.* **1994**, *98*, 13513. Singer, K. D.; Lalama, S. L.; Sohn, J. E.; Small, R. D.; *Nonlinear Optical Properties of Organic Molecules and Crystals*; Chemla, D. S., Zyss, J., Ed.; Academic Press: New York, 1987; Vols. 1 and 2.

(27) Lewis, J. E.; Maroncelli, M. *Chem. Phys. Lett.* **1998**, *282*, 197.

(28) Maroncelli, M.; Fleming, G. R. *J. Chem. Phys.* **1987**, *86*, 6221.

(29) Liptay, W. Dipole moments and polarizabilities of molecules in excited states. In *Excited States*; Lim, E. C., Ed.; Academic Press: New York, 1974; pp 129−229.

(30) Locknar, S. A.; Peteanu, L. A.; Shuai, Z. *J. Phys. Chem. A* **1999**, *103*, 2197.

(31) The values of $|\Delta\vec{\mu}|$ and $\overline{\Delta\alpha}$ in ref 9 are also reported in units of $Å^3/f_c^2$ and D/f_c, respectivlely, and not in units of $f_c^2Å^3$ and f_cD, as inaccurately transcribed.

(32) Fonseca Guerra, C.; Snijders, J. G.; te Velde, G.; Baerends, E. J. *Theor. Chem. Acc.* **1998**, *99*, 391. van Gisbergen, S. J. A.; Snijders, J. G.; Baerends, E. J. *J. Comput. Phys. Commun.* **1999**, *118*, 119.

(33) Becke, A. D. *J. Chem. Phys.* **1986**, *84*, 4524.

(34) Lee, C.; Yang, W.; Parr, R. *Phys. Rev. B* **1998**, *37*, 785.

(35) Borgstahl, G. E. O.; Williams, D. R.; Getzoff, E. D. *Biochemistry* **1995**, *34*, 6278.

(36) Getzoff, E. D.; Gutwin, K. N.; Genick, U.K. *Nat. Struct. Biol.* **2003**, *10*, 663.

(37) The absolute values of the ground and excited-state dipole moments of the anions depend on the location of the origin, although the magnitudes of the difference dipole moments themselves are un-affected. Here, the origin is set at the centre of mass of the molecule.

(38) Frank, I.; Hutter, J.; Marx, D.; Parrinello, M. *J. Chem. Phys.* **1998**, *108*, 4060. Filatov, M.; Shaik, S. *Chem. Phys. Lett.* **1998**, *288*, 689.

(39) Hutter, J.; et al., Copyright IBM Corp 1990−2001, Copyright MPI für Festkörperforschung Stuttgart 1997−2001.

(40) Frisch, M. J.; Trucks, G. W.; Schlegel, H. B.; Scuseria, G. E.; Robb, M. A.; Cheeseman, J. R.; Zakrzewski, V. G.; Montgomery, J. A., Jr.; Stratmann, R. E.; Burant, J. C.; Dapprich, S.; Millam, J. M.; Daniels, A. D.; Kudin, K. N.; Strain, M. C.; Farkas, O.; Tomasi, J.; Barone, V.; Cossi, M.; Cammi, R.; Mennucci, B.; Pomelli, C.; Adamo, C.; Clifford, S.; Ochterski, J.; Petersson, G. A.; Ayala, P. Y.; Cui, Q.; Morokuma, K.; Malick, D. K.; Rabuck, A. D.; Raghavachari, K.; Foresman, J. B.; Cioslowski, J.; Ortiz, J. V.; Stefanov, B. B.; Liu, G.; Liashenko, A.; Piskorz, P.; Komaromi, I.; Gomperts, R.; Martin, R. L.; Fox, D. J.; Keith, T.; Al-Laham, M. A.; Peng, C. Y.; Nanayakkara, A.; Gonzalez, C.; Challacombe, M.; Gill, P. M. W.; Johnson, B. G.; Chen, W.; Wong, M. W.; Andres, J. L.; Head-Gordon, M.; Replogle, E. S.; Pople, J. A. *Gaussian 98*, revision A.6; Gaussian, Inc.: Pittsburgh, PA, 1998.

(41) Böttcher, C. J. F. *Theory of Electric Polarisation*; Elsevier Publishing Co.: Amsterdam, 1952; p 492.

(42) Liptay, W.; Becker, J.; Wehning, D.; Lang, W.; Burkhard, O. *Z. Naturforsch* **1982**, *37a*, 1396.

(43) Bublitz, G. U.; Boxer, S. G. *J. Am. Chem. Soc.* **1998**, *120*, 3988.

(44) The partial atomic charges for a model-pG type system previously presented[21]utilizes different methods to evaluate ground- and excited-state charges, and can significantly affect the magnitudes of the charge differences.

(45) Demchuk, E.; Wade, R. *J. Phys. Chem.* **1996**, *100*, 17373.

(46) Imamoto, Y.; Kataoka, M.; Tokunaga, F. *Biochemistry* **1996**, *35*, 14047. Zhou, Y.; Ujj, L.; Meyer, T. E.; Cusanovich, M. A.; Atkinson, G. H. *J. Phys. Chem. A* **2001**, *105*, 5719.

(47) Blanchard, G. J.; Jiang, Y.; McCarthy, P. K. *Chem. Phys.* **1994**, *183*, 249.